

Analysis of Beauty Production and Hadronization in Vacuum and Quark-Gluon Plasma with CMS

by

Zhaozhong Shi

B.A., University of California, Berkeley (2016)

Submitted to the Department of Physics
in partial fulfillment of the requirements for the degree of

Doctor of Philosophy in Physics

at the

MASSACHUSETTS INSTITUTE OF TECHNOLOGY

September 2021

© Massachusetts Institute of Technology 2021. All rights reserved.

Author
Department of Physics
September 5, 2021

Certified by
Yen-Jie Lee
Associate Professor
Thesis Supervisor

Accepted by
Nergis Mavalvala
Associate Department Head of Physics

Analysis of Beauty Production and Hadronization in Vacuum and Quark-Gluon Plasma with CMS

by

Zhaozhong Shi

Submitted to the Department of Physics
on September 5, 2021, in partial fulfillment of the
requirements for the degree of
Doctor of Philosophy in Physics

Abstract

A novel analysis of fully reconstructed B_s^0 , B^0 , and B^+ mesons decay into J/ψ and strange hadrons using Compact Muon Solenoid (CMS) Experiment 2017 pp dataset and 2018 PbPb data at the center of mass energy per nucleon $\sqrt{s_{NN}} = 5.02$ TeV at the Large Hadron Collider (LHC) is presented in this thesis. We apply machine learning techniques to obtain significant B-meson signals and extend the kinematic regime of B-meson measurements. In our analysis, B_s^0 signal of greater than 5σ significance is first confirmed in heavy-ion collisions. The inclusive beauty production cross section in pp collisions from the B^+ exclusive decay cross section down to zero transverse momentum is measured. The precise measurement of B-meson nuclear modification factor and B_s^0/B^+ ratio and the comparisons with theoretical model predictions will also be discussed. Our results will help elucidate the beauty production and hadronization mechanisms in vacuum and quark-gluon plasma at the LHC energy.

Thesis Supervisor: Yen-Jie Lee

Title: Associate Professor

Acknowledgments

This is the acknowledgements section. You should replace this with your own acknowledgements.

Contents

1	Introduction	17
1.1	The Standard Model of Particle Physics	17
1.2	Quantum Chromodynamics	18
1.2.1	QCD Lagrangian	18
1.2.2	Asymptotic Freedom	19
1.2.3	Perturbative QCD	20
1.2.4	Non-perturbative QCD	21
1.2.5	QCD Factorization Theorem	21
1.2.6	Color Confinement	22
1.2.7	Hadronization	22
1.3	QCD In Extreme Conditions	23
1.3.1	QCD at Finite Temperature	23
1.3.2	Melting of QCD Vacuum	24
1.3.3	Chiral Symmetry Restoration	24
1.3.4	Temperature Dependence of QCD Static Potential	26
1.3.5	Hadron Mass Spectrum and Hagedorn Temperature	27
1.3.6	Color Deconfinement	28
1.3.7	QCD at High Parton Density	28
1.3.8	Color Glass Condensate	28
1.3.9	Nuclear Shadowing	29
1.4	QCD Matter	29
1.4.1	QCD Phase Diagram	29

1.4.2	Hadron Resonance Gas	30
1.4.3	Quark-Gluon Plasma	32
1.4.4	Color Superconductor	33
1.4.5	Phase Transition	33
1.4.6	Critical Point	34
1.5	High Energy Nuclear Physics	34
1.5.1	Laboratories	34
1.5.2	Heavy-Ion Accelerators	35
1.5.3	Heavy-ion Physics Detectors	35
1.5.4	Stages of Heavy-Ion Collisions	35
1.5.5	Coordinates	35
1.5.6	Glauber Model	35
1.6	The Quest for the Quark-Gluon Plasma	35
1.6.1	Signatures	35
1.6.2	Discovery	35
1.6.3	Properties	35
1.6.4	Microscopic Structure	35
1.6.5	Open Questions	35
1.7	Hard Probes	35
1.7.1	Jets	35
1.7.2	Electroweak Probes	35
1.7.3	Heavy Quarks	35
1.8	Open Heavy Flavor Physics	35
1.8.1	Heavy Quark Diffusion	35
1.8.2	Heavy Quark Energy Loss	35
1.8.3	Heavy Quark Hadronization	35
1.8.4	Experimental Observables	35
2	The CMS Detector	37
2.1	Overview	38

2.2	Triggers	38
2.2.1	L1 Hardware Trigger	38
2.2.2	HLT Trigger	38
2.3	Tracking System	38
2.3.1	Silicon Pixel Detector	38
2.3.2	Silicon Strip Detector	38
2.3.3	Tracking Algorithm	38
2.4	Muon System	38
2.5	Calorimeter System	38
2.5.1	ECAL	38
2.5.2	HCAL	38
2.5.3	Forward HCAL	38
3	Experimental Procedures	39
3.1	Experimental Setup	39
3.2	LHC Heavy-Ion Run	39
3.3	Minimum Biased Trigger	39
3.4	Dimuon Trigger	39
3.5	Run Monitoring	39
3.6	Data Acquisition	39
4	Technical Objects	41
4.1	Hits	41
4.2	Clusters	41
4.3	Tracks	41
4.4	Vertices	41
4.5	Muons	41
5	Data Analysis	43
5.1	Analysis Strategies	44
5.1.1	Physics Goals	44

5.1.2	General Workflow	44
5.1.3	Technical Challenges	44
5.2	Global Event Observables	44
5.2.1	Total Number of Events	44
5.2.2	Centrality Definition	44
5.2.3	Number of Participants Nucleons	44
5.2.4	Number of Binary Collisions	44
5.2.5	Event Multiplicity	44
5.3	Monte Carlo Simulations	44
5.3.1	PYTHIA	44
5.3.2	Hydjet Embedding	44
5.3.3	EvtGen Package	44
5.3.4	Reweighting	44
5.4	B meson Reconstruction	44
5.4.1	Decay Channels	44
5.4.2	Event Selections	44
5.4.3	Track and Muon Selections	44
5.4.4	Results	44
5.5	Cut Optimization	44
5.5.1	Topological Variables	44
5.5.2	Multivariate Analysis	44
5.5.3	Machine Learning Techniques	44
5.5.4	Training Performance	44
5.5.5	Working Point Determination	44
5.6	Signal Extraction	44
5.6.1	B-meson Invariant Mass Distributions	44
5.6.2	Fitting Models	44
5.6.3	Raw Yield Extraction	44
5.6.4	Signal Significance Estimation	44
5.7	Acceptance and Efficiency Correction	44

5.7.1	Analysis Challenges	44
5.7.2	Fiducial Measurement	44
5.7.3	Fine 2D Efficiency Map	44
5.7.4	Data-Drive Efficiency Correction	44
5.7.5	Tag & Probe Techniques	44
5.7.6	Nominal Results	44
5.8	Cross Section Results	44
5.9	Validation Tests	44
5.9.1	Mass Scraping Test	44
5.9.2	Raw Yield Closure	44
5.9.3	Efficiency Closure	44
5.9.4	sPlot Closure	44
5.10	Statistical Uncertainties Determination	44
5.10.1	Data Bootstrapping	44
5.10.2	Statistical Uncertainties Interpretation	44
5.11	Systematic Uncertainties Estimation	44
5.11.1	Global Observables	44
5.11.2	Branching Ratios	44
5.11.3	Tracking Efficiency	44
5.11.4	Muon Efficiency	44
5.11.5	Selection Efficiency	44
5.11.6	Signal Extraction	44
5.11.7	Summary	44
5.12	Final Results	44
5.12.1	B_s^0 and B^+ Cross Section	44
5.12.2	B_s^0/B^+ Ratio	44
5.12.3	B_s^0 and B^+ Nuclear Modification Factor	44
6	Conclusions	45
6.1	Comparison with Other Experiments and Theoretical Models	45

6.2	Physics Messages Discussion	45
6.3	Conclusions	45
6.4	Future Outlooks	45
7	Other Studies	47
7.1	sPHENIX Heavy Flavor Physics Simulations	47
7.2	sPHENIX Electromagnetic Calorimeter Studies	47
7.3	EIC Electromagnetic Calorimeter R&D	47
A	Tables	49
B	Figures	51
	List of Symbols	55
	Abbreviations	57

List of Figures

1-1	The 17 elementary particles, including leptons, quarks, gauge bosons, and Higgs boson, and their basic properties, such as mass, electric charge, spin, in the Standard Model of Particles Physics are shown above.	18
1-2	The running of the strong coupling constant α_s in different experiments at different energy scale Q and the comparison with QCD calculations are shown above.	20
1-3	The QCD factorization theorem applied to a pp collision event involving in soft and hard processes are shown above.	21
1-4	The fragmentation process of charms quarks hadronize into D^\pm (left) and the coalescence process of beauty quark with a strange quark nearby to form a B_s^0 are shown above.	23
1-5	Many-body dynamics of QCD in different physics limits is shown above.	23
1-6	The Feynman diagram of a triangular quark loop under external magnetic field B describe the generation of chiral magnetic current via chiral anomaly is shown above.	25
1-7	The schematics of charge separation due chirality imbalance of quarks under a strong magnetic field in heavy-ion collisions, know as Chiral Magnetic Effect, is shown above.	26
1-8	The P-T diagram of water in gas, liquid, solid phases is shown above.	29

1-9	The theoretical QCD phase diagram of different QCD matter, including hadron resonance gas, quark-gluon plasma, neutron star, and color superconductor, as function of temperature and baryon chemical potential is shown above. The solid line indicates the conjecture of first order phase transition between quark-gluon plasma and hadron gas while the dash line is a smooth crossover.	30
1-10	The schematic plot of potential energy between two nucleon via pion exchange as a function of distance is shown above [43]. This potential with a well minimizing near 100 MeV allow nucleons to bind together and form atomic nuclei and nuclear matter.	31
1-11	The pressure and energy density from lattice simulation compared with ideal hadron resonance gas and Van der Waas interaction at different $\frac{\mu_B}{T}$ are shown above.	31
B-1	Armadillo slaying lawyer.	51
B-2	Armadillo eradicating national debt.	52

List of Tables

A.1	Armadillos	49
-----	----------------------	----

Chapter 1

Introduction

1.1 The Standard Model of Particle Physics

Physics is the research of relationship between space and time and energy and matter. Physicists enjoy searching for symmetries and consideration laws in nature. They develop elegant mathematical formulations to describe the beauty of the nature and predict or explain the experimental results and observed phenomena.

There are four known fundamental forces in nature: gravitational force, electromagnetic force, strong force, and weak force. The gravitation force describes the interaction between two massive objects. The electromagnetic force describe the interaction between electrically charged objects. The strong force describes the interaction between nucleons. The weak force describe the radioactive decay of particles. The Standard Model (SM) of Particle Physics is based on theoretical of relativistic quantum field theory with a gauge symmetry of $SU(3) \times SU(2) \times U(1)$ [1]. It unifies the strong, weak, and electromagnetic into a single theory and describes all particles participating in these interactions. The ingredient of the standard model are lepton, quarks, gauge boson, and Higgs boson shown in Figure 1-1.

There are 19 parameters in the Standard Model: 6 quark masses, 3 lepton masses, 3 coupling strengths, 4 CKM angles, Higgs mass, vacuum expectation value, and QCD vacuum angle. These parameters are determined from the experiments. Physicists perform calculations based on the Standard Model and predict the cross section

mass →	2.4 MeV/c ²	1.27 GeV/c ²	171.2 GeV/c ²	0	≈126 GeV/c ²
charge →	2/3	2/3	2/3	0	0
spin →	1/2	1/2	1/2	1	0
	u up	c charm	t top	γ photon	H Higgs boson
QUARKS					
	4.8 MeV/c ²	104 MeV/c ²	4.2 GeV/c ²	0	
	-1/3	-1/3	-1/3	0	
	1/2	1/2	1/2	1	
	d down	s strange	b bottom	g gluon	
	0.511 MeV/c ²	105.7 MeV/c ²	1.777 GeV/c ²	91.2 GeV/c ²	
	-1	-1	-1	0	
	1/2	1/2	1/2	1	
	e electron	μ muon	τ tau	Z Z boson	
LEPTONS					
	<2.2 eV/c ²	<0.17 MeV/c ²	<15.5 MeV/c ²	80.4 GeV/c ²	
	0	0	0	±1	
	1/2	1/2	1/2	1	
	ν_e electron neutrino	ν_μ muon neutrino	ν_τ tau neutrino	W W boson	
					GAUGE BOSONS

Figure 1-1: The 17 elementary particles, including leptons, quarks, gauge bosons, and Higgs boson, and their basic properties, such as mass, electric charge, spin, in the Standard Model of Particles Physics are shown above.

of different processes in high energy physics experiments. Since it is proposed in the 1970s, the Standard Model has been tested extensively in countless high-energy physics experiments. Its prediction holds for all of them with very few exceptions. The Standard Model consists of two sectors: the Electroweak theory (EW) and Quantum Chromodynamics (QCD). The Lagrangian of the Standard Model can be written as the sum of EW and QCD: $\mathcal{L}_{SM} = \mathcal{L}_{EW} + \mathcal{L}_{QCD}$

1.2 Quantum Chromodynamics

1.2.1 QCD Lagrangian

QCD, a non-abelian gauge theory with $SU(3)$ symmetry, is the theory for the strong interaction between quarks and gluons. The QCD Lagrangian is as follows:

$$\mathcal{L}_{QCD} = \bar{\Psi}^i i(\not{D})_{ij} \Psi^j - m \bar{\Psi}^i \Psi_i - \frac{1}{16\pi^2} G_a^{\mu\nu} G_{\mu\nu}^a \quad (1.1)$$

Where

$$\not{D} = \gamma^\mu \partial_\mu - ig_s \frac{\lambda}{2} \gamma^\mu A_\mu \quad (1.2)$$

$$G_a^{\mu\nu} = \partial^\mu A_a^\nu - \partial^\nu A_a^\mu + g_s f_{abc} A_b^\mu A_c^\nu \quad (1.3)$$

Here, λ are the Gell-Mann Matrices. f_{abc} is the structure of constant of $SU(3)$. A^μ is the eight gluon field. g_s is the strong coupling constant. The color indices i and j run from 1 to 3, which stands for 3 colors: red, blue, and green. The gluon field indices a , b , and c run from 1 to 8, standing for the 8 gluon state (Gluon octet as the combination of 3 color and 3 anticolor: $3 \times \bar{3} = 1 \oplus 8$) living in the adjoint representation of $SU(3)$ of color.

1.2.2 Asymptotic Freedom

The running of the strong coupling constant $\alpha_s = \frac{g_s^2}{4\pi}$ according to the 1-loop calculations in the renormalization theory [2] is shown as follows

$$\alpha_s(Q^2) = \frac{12\pi}{(11N_c - 2N_f) \ln(\frac{Q^2}{\Lambda_{QCD}^2})} \quad (1.4)$$

We can see that as the energy scale increases, the coupling strength of the strong interaction decreases. This is in contrast to QED where the electromagnetic coupling strength increases as the energy scale increases. In the ultra-violet limit $Q^2 \rightarrow \infty$ and $\alpha_s \rightarrow 0$, quarks and gluons behave like free particles. This feature in QCD is called Asymptotic Freedom [4]. Meanwhile, in the infrared limit, the strong coupling constant increases. Near the $\Lambda_{QCD} \simeq 100$ MeV, the coupling is greater than 1, where the perturbative expansion of QCD breaks down. Experimentally, physicists measure the strong coupling constant at different energy scales from different experiments at different colliders. Figure 1-2 [3] show the running of strong coupling constant in experiment and comparison with the theoretical calculations

An excellent agreement between the theoretical predictions and experimental results of the strong coupling constant is observed in Figure 1-2.

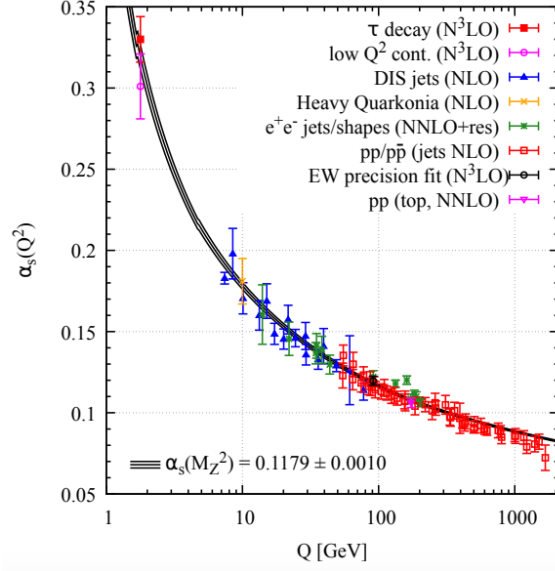


Figure 1-2: The running of the strong coupling constant α_s in different experiments at different energy scale Q and the comparison with QCD calculations are shown above.

1.2.3 Perturbative QCD

It is mathematically proven that there is in general no closed form expression for the Standard Model Lagrangian under the Quantum Field Theory framework. Therefore, physicist develop perturbation theory in Quantum Field Theory and apply it to the Standard Model. Physicist obtain asymptotic expansions as power series of the coupling constants and approximately calculate the expectation values of the observables to prediction experimental results.

For QCD, in high energy and hard scattering processes, since the coupling constant is much less than 1, perturbation theory is applicable to QCD. Feynman rules and diagrams are applicable in the matrix element to evaluate the cross section of hard parton-parton scattering. Perturbative QCD (pQCD) calculations have been tested various experiments such as electron positron annihilation, deep inelastic electron proton scattering, and high energy proton-proton collisions.

1.2.4 Non-perturbative QCD

At low energy and soft scattering processes, the coupling constant is greater than 1, perturbation theory of QCD breaks down. Many low-energy QCD processes such as hadronization and hadron-hadron interactions are non-perturbative. Historically, physicists developed Lattice gauge theory such as Lattice QCD to calculate the mass [5] of the proton and effective theory such as Chiral Perturbation Theory to study pion-nucleon scattering [6]. Non-perturbative QCD have achieved many successes. Currently, many novel developments applying non-perturbative QCD to understand nuclear structure and nucleon spin structure are being carried by physicists.

1.2.5 QCD Factorization Theorem

The QCD factorization theorem states that in events involving both hard and soft QCD processes, hard and soft process are mathematically factorized in the cross section computation as follows [7]:

$$\sigma_X = \Sigma \int dx_1 dx_2 f_i(x_1, \mu_F^2) f_j(x_2, \mu_F^2) \times \hat{\sigma}_{ij \rightarrow X}(p_1, p_2, \mu_R^2, \mu_F^2) \quad (1.5)$$

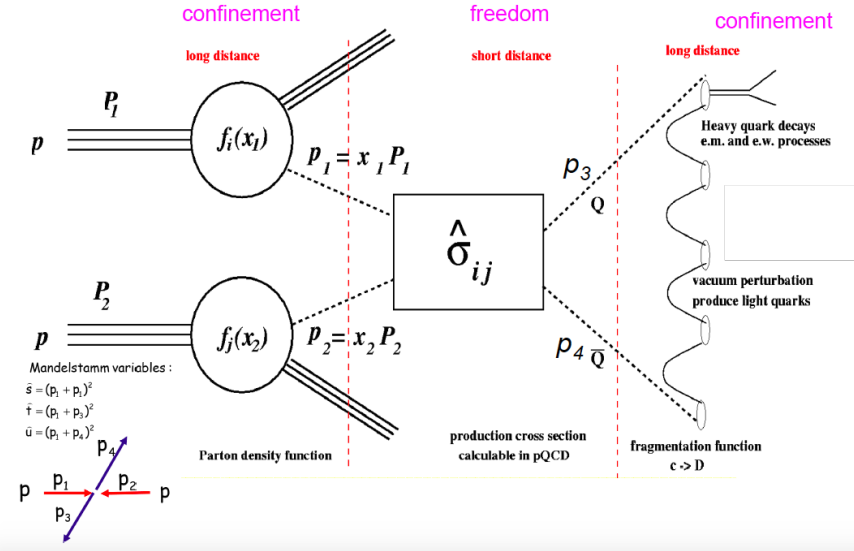


Figure 1-3: The QCD factorization theorem applied to a pp collision event involving in soft and hard processes are shown above.

The hard processes are encoded in the factor of partonic cross sections while the soft processes are measured in experiments. Physicists developed parton distribution function to describe initial kinematic of partons inside hadrons and fragmentation function to describe the parton hadronization process. Both parton distribution function and fragmentation function are measured in experiments.

Physicists apply QCD factorization theorem to perform pQCD calculation of hard scattering processes and use the measurement from the to understand the hadron spectroscopy in electron-positron, electron-proton, and proton-proton collisions.

1.2.6 Color Confinement

Another feature of QCD as a non-abelian gauge theory is color confinement. The strong force carrier gluon itself is also color charged. Color charged partons, namely quarks and gluons, are never detected in isolation. In experiments, only color neutral hadrons are detected. Currently, the analytic explanation of color confinement is still not yet rigorously proven. The theoretical explanation of color confinement in QCD remains one of the unsolved problem in physics.

1.2.7 Hadronization

The formation process hadrons from partons is called hadronization. Because in experiments we only measure final state hadrons, in order to study the interactions and dynamics of quarks and gluons during partonic stage from hadron spectra, we also need to understand hadronization mechanisms. However, hadronization is in general non-perturbative and cannot yet be described by first principle QCD calculations. Therefore, physics make phenomenological models such as the Statistical Hadronization Model [8], Lund String Model [9], Quark Coalescence Model [10] to study hadronization. Figure 1-4 shows the schematics of hadronization of a beauty quark via fragmentation and coalescence process.

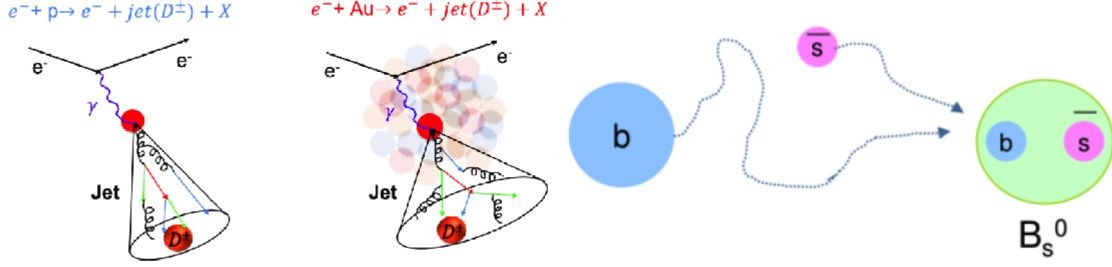


Figure 1-4: The fragmentation process of charms quarks hadronize into D^\pm (left) and the coalescence process of beauty quark with a strange quark nearby to form a B_s^0 are shown above.

1.3 QCD In Extreme Conditions

Historically, many efforts to understand QCD in extreme conditions have been made [11]. There are mainly two directions: temperature and parton density. Figure 1-5 shows the different studies of QCD in different conditions [12]:

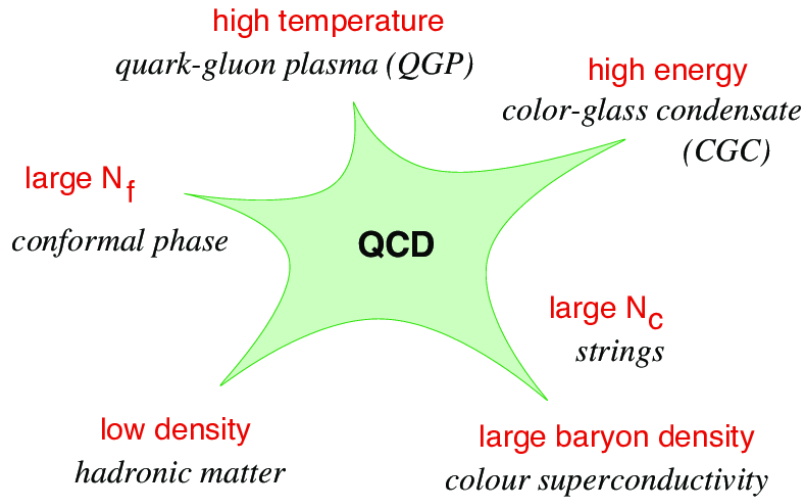


Figure 1-5: Many-body dynamics of QCD in different physics limits is shown above.

1.3.1 QCD at Finite Temperature

In QCD, under extremely high energy density, the degree of freedom of the system increases via particle production. Many-body dynamics become relevant. In the

limit of large number of quarks and gluons, after a sufficiently long period of time, the system reach thermal equilibrium via strong interaction [13–15]. Therefore, a description based on thermodynamics can be formulated to study such systems [17]. We call this thermalized and strongly interacting many-body system of quarks and gluons to be QCD matter.

Therefore, an additional variable temperature (**T**) can be introduced to study such QCD systems. There are some interesting QCD phenomenologies involving temperature as listed in the following subsections.

1.3.2 Melting of QCD Vacuum

The QCD vacuum is filled with various condensates of quarks-antiquark pair and gluon fields [16]. In the QCD vacuum, the three flavor of light quarks: u , d , s form a flavor symmetry group of $SU(3)_f$. However, for quark-quark pair, the $SU(3)_f \times SU(3)_f$ chiral symmetry is spontaneously broken. For example, in the vacuum, a quark-antiquark pair field has a non-vanishing expectation value of $\langle 0 | \bar{\psi}(x)\psi(x) | 0 \rangle \simeq (250 \text{ MeV})^3$ []. Therefore, in the physical QCD vacuum, all color field are confined in hadrons. In 1974 T.D. Lee formulated the idea that the non-perturbative vacuum condensates could be “melted down ... by distributing high energy or high nucleon density over a relatively large volume” [18, 19]. As the energy density in space increases, the color field start to permeate all space. This is effective melting the QCD Vacuum as the temperature of the system increases. Therefore, the temperature of the system will affect the QCD vacuum structure.

1.3.3 Chiral Symmetry Restoration

At a finite critical temperature $T_c > 0$, the quark-antiquark pair field will have a vanishing expectation value. In this scenario, massive quarks behave as if massless [22]. Thus, the chiral symmetry of quarks is restored [23]. Therefore, under a strong magnetic field, due to the restored chiral symmetry, the quarks generate anomalous chiral current j_5^μ described by $U(1)_A$ chiral anomaly, calculated by the famous “Triangle

Feynman diagram" in Figure 1-6 shown below:

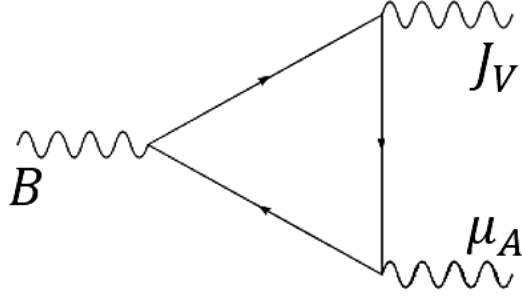


Figure 1-6: The Feynman diagram of a triangular quark loop under external magnetic field B describe the generation of chiral magnetic current via chiral anomaly is shown above.

The anomalous chiral current $j^{\mu 5}$ is given by [24]

$$\partial_\mu j_5^\mu = -\frac{N_f g^2}{16\pi^2} G_a^{\mu\nu} \widetilde{G}_{\mu\nu}^a \quad (1.6)$$

Here $G_a^{\mu\nu}$ is defined as

$$\widetilde{G}_{\mu\nu}^a = \frac{1}{2} \epsilon_{\mu\nu\lambda\sigma} G^{\lambda\sigma a} \quad (1.7)$$

According to the continuity equation of chiral current

$$\frac{\partial \rho_5}{\partial t} + \nabla \cdot \vec{j}_5 = 0 \quad (1.8)$$

By definition, the chiral current ρ_5 is the difference of the right-handed charge ρ_L and left-handed charge ρ_R .

In terms of number of particles $N_5 = \frac{Q_5}{e} = \int \rho_5 d^3x$, integrating both sides by the spatial volume and divide by the volume, we have

$$\frac{dN_5}{dt} = \int d^3x \nabla \cdot \vec{j}_5 = \int -\frac{N_f g^2}{16e\pi^2} G_a^{\mu\nu} \widetilde{G}_{\mu\nu}^a d^3x \quad (1.9)$$

The chiral chemical potential μ_5 is proportional to the number of particle N_5 : $j_5 \propto N_5$ This non-vanishing anomalous chiral current implies non-zero chiral magnetic

dipole moment density $\mu_5 \neq 0$. Finally, under an external magnetic field, the induced electric current j_V^μ is given by

$$\vec{J}_V = \frac{N_c e}{2\pi^2} \mu_A \vec{B} \neq 0 \quad (1.10)$$

In experiments, we should expect to see the separation of left-handed and right-handed quarks Q_V due to this electric current \vec{J}_V where charge imbalance between the positive and negative direction along the magnetic field [25] as $\Delta Q = \int_0^\tau \vec{J}_V \cdot \vec{A} dt \neq 0$. We call this chirality imbalance effect due to the restored chiral symmetry of quarks at finite temperature as **Chiral Magnetic Effect** [26]. Figure 1-7 illustrates the schematics of Chiral Magnetic Effect in Heavy-Ion Collisions [27]

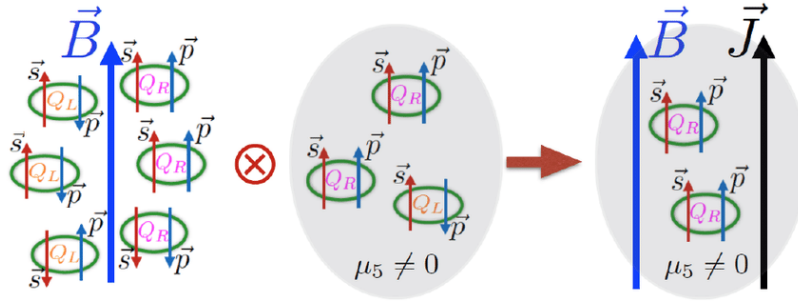


Figure 1-7: The schematics of charge separation due to chirality imbalance of quarks under a strong magnetic field in heavy-ion collisions, known as the Chiral Magnetic Effect, is shown above.

Currently, physicists are actively looking for evidence of the Chiral Magnetic Effect in experiments but have not yet reported any conclusive results so far [28].

1.3.4 Temperature Dependence of QCD Static Potential

If we consider two quarks in the limit of finite mass and are essentially at rest in the lab frame, we can define a QCD static potential between these two quarks due to the strong interaction. In vacuum, such a potential is called “Cornell Potential” [20]. The potential as a function of the distance between two quarks is shown as follows:

$$V(r) = -\frac{\alpha_{eff}}{r} + \sigma r \quad (1.11)$$

Here, α_{eff} is the effective strong coupling coupling between the two quarks and $\sigma \simeq 0.184 \text{ GeV}/c$ is the string coupling constant [?].

Now if we consider at finite temperature T with a thermalized system between the two quarks, the QCD static potential becomes:

$$V(r) = -\frac{\alpha_{eff}}{r}e^{-m_D r} + \frac{\sigma}{m_D}(1 - e^{-m_D r}) \quad (1.12)$$

Here, $m_D \sim g_s T$ is the Debye mass due to Debye color screening effect [21], which essentially modifies the gluon propagator by inserting a finite mass term: $-i\frac{g^{\mu\nu}}{q^2} \rightarrow -i\frac{g^{\mu\nu}}{q^2 - m_D^2}$. In fact, Equation (2) reduces to the Cornell potential when $T = 0$. The QCD static potential is shown below in Figure ??

Many interesting physics implications can be deduced from QCD at finite temperature.

1.3.5 Hadron Mass Spectrum and Hagedorn Temperature

In 1965, Hagedorn proposed a statistical thermodynamically bootstrap model, giving the temperature dependence of hadron spectra [29]. According to the principle of asymptotic bootstrap, in the limit of high mass resonance $m \rightarrow \infty$ the mass spectrum of hadrons $\rho(m)$ grows exponentially

$$\rho(m) \propto m^{-\frac{5}{2}} e^{\frac{m}{T_0}} \quad (1.13)$$

Here, $\rho(m) dm$ stands for the number of excited hadron with mass between m and $m + dm$. $T_0 \simeq 158 \text{ MeV}$ is the temperature parameter extract from experiments. As $T \rightarrow T_0^-$, $\rho(m) \rightarrow \infty$. The mass spectrum of hadrons diverges. Therefore, it stands for the highest possible temperature achievable for the strong interaction between hadrons. Hence, T_0 is also called the ‘‘Hagedorn Temperature’’. For $T > T_0$, the description of color-neutral hadrons mass spectrum will break down, indicating a

new type of matter with deconfined degree of freedom in the interaction [30].

1.3.6 Color Deconfinement

As mentioned in the sections above, we see that, at finite temperature, the QCD static potential is screened and color degree of freedom become relevant in the system. As the temperature of the system increase, the quarks and gluon inside color-neutral hadrons will have more available space to move around and start to deconfine [31]. At some critical temperature T_c , quarks and gluons will form a new type color deconfined QCD matter, which is called Quark-Gluon Plasma (QGP). The typical temperature of QGP is in the order of a few hundred MeV or about 10^{12} K, which is about a million times hotter than the core of the Sun.

1.3.7 QCD at High Parton Density

In the other direction, while keeping zero temperature, by increasing density of the color fields of the system, another form of QCD matter will also emerge [32]. Due to confinement, a single quark or gluon cannot exit in vacuum. Therefore, the simplest form of QCD system will be a meson, which consist of one quark and one antiquark. The next more complex system will be baryon, for instances, nucleons, which consist of three quarks. We can then use nucleons to form atomic nuclei and even neutron stars. As the number of nucleons in the system increases, the nucleon density also increases, which increase the color field density. Below, we will discuss the consequence of increasing color field density by increasing the color field lines and decreasing the volume of the system. In general, we can study QCD at High Parton Density by probing small- x physics [33]

1.3.8 Color Glass Condensate

One way to increase the color field density is by decreasing its volume. The radius of a hadron will shrink due to the Lorentz contraction effect as it moves with respect to the spectator. However, since the number of color charges inside the does not

change, the color field density will increase. At very high energy, the hadrons will turn into “gluon walls” [34] and form a dense color field of matter [35] named Color Glass Condensate is formed [36].

1.3.9 Nuclear Shadowing

At high energy, or equivalently, small x , according to the QCD evolution equation, the gluons inside the nucleon of the nuclei will “create shadows” on each other [37], The high density effects results in the modification of the nuclear structure function and the gluon nucleon parton distribution [38]. Therefore, in high energy hadron-nucleus collision, we expect to see the decrease of cross section per participant nucleons at small- x region compared other x region [39]. We call this effect as “nuclear shadowing (of gluons)” [42].

1.4 QCD Matter

1.4.1 QCD Phase Diagram

Similar to form everyday matters such as metal, water, wood, glass, and plastic, which are formed by electromagnetic interaction and could all be described macroscopically by equations of states that are parameterized by thermodynamic variables. Figure 1-8 shows the phase diagram of water (H_2O) at different temperature and pressure:

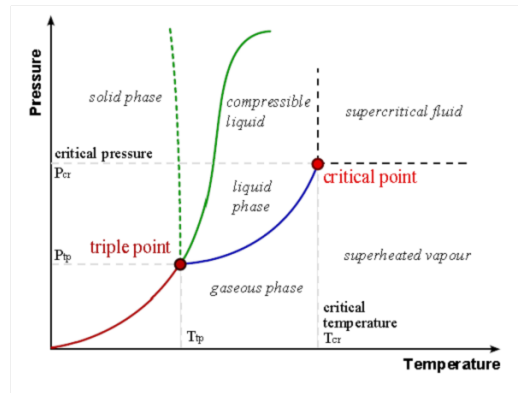


Figure 1-8: The P-T diagram of water in gas, liquid, solid phases is shown above.

Similarly, QCD matter is the matter formed by numerous quarks and gluons via the strong interaction and can also be describe by equations of states. Like our everyday matter which has gas, liquid, and solid phases at different pressure and temperature, QCD matter also has different phases at different temperature and baryon chemical potential. and can be describe by QCD phase diagrams. Figure 1-9 shows the QCD phase diagram at different temperature and baryon chemical potential:

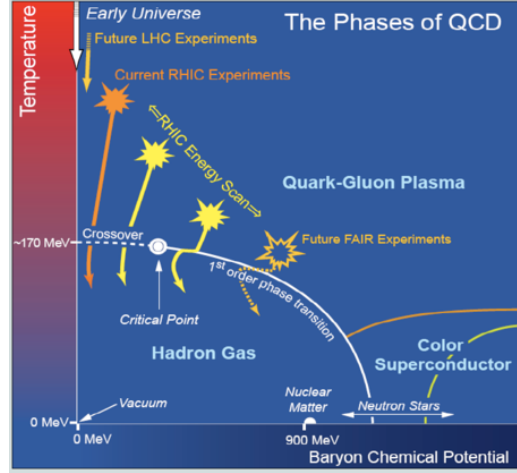


Figure 1-9: The theoretical QCD phase diagram of different QCD matter, including hadron resonance gas, quark-gluon plasma, neutron star, and color superconductor, as function of temperature and baryon chemical potential is shown above. The solid line indicates the conjecture of first order phase transition between quark-gluon plasma and hadron gas while the dash line is a smooth crossover.

1.4.2 Hadron Resonance Gas

One of the most familiar type of QCD matter is hadron resonance gas, which lies at the left bottom corner of the QCD phase diagram. Hadron resonance gas is a system of color neutral hadrons at relative low temperature. The interaction between hadrons are the Van der Waas like strong nuclear force as the residue of the color force via exchange of mesons. The strong nuclear force between two nucleons shown below Figure 1-10.

The equation of state of non-interacting hadron resonance gas could be described by grand canonical ensemble of bosons (mesons) and fermions (baryons) [40]. We

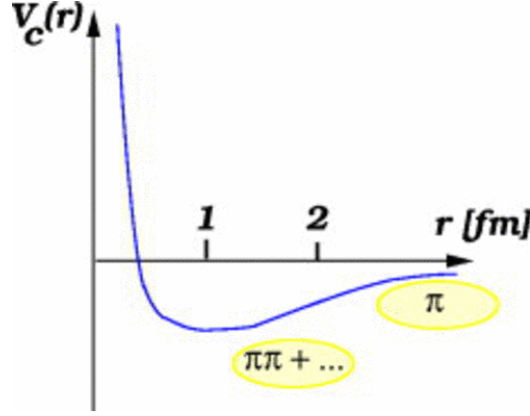


Figure 1-10: The schematic plot of potential energy between two nucleon via pion exchange as a function of distance is shown above [43]. This potential with a well minimizing near 100 MeV allow nucleons to bind together and form atomic nuclei and nuclear matter.

should note that pions dominates the hadron gas at low temperature. The realistic equation of state of hadron resonance gas should also consider the interaction. An example of the equation of state of hadron resonance gas consider the Van der Waas interaction comparing with lattice QCD simulation is given in Figure 1-11 below [41]:

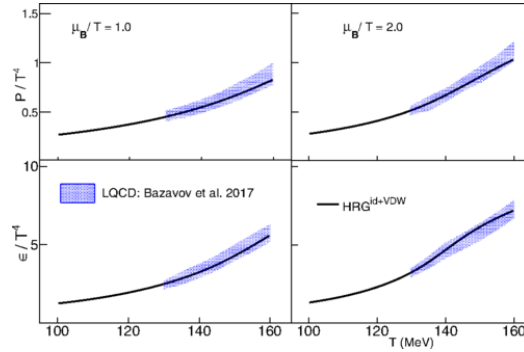


Figure 1-11: The pressure and energy density from lattice simulation compared with ideal hadron resonance gas and Van der Waas interaction at different $\frac{\mu_B}{T}$ are shown above.

Nuclear matter is considered as part of the hadron resonance gas in the QCD phase diagram. Examples of typical hadron gas will be atomic nuclei at a famous nuclear matter saturation density $n_S = 0.16 \text{ fm}^{-3}$ (baryon density $n_B = 3n_S$) and nuclear matter like neutron star at large baryon density.

1.4.3 Quark-Gluon Plasma

At very high temperature, quarks and gluons inside the color neutral hadron resonance gas will deconfine and form a new type of matter called quark-gluon plasma (QGP). In cosmology, it is believed that QGP exists in the early universe just several microseconds after the Big Bang during the quark epoch after electroweak phase transition and before nucleosynthesis [44].

The temperature of QGP is in order of hundreds of MeV, which is about a million times hotter than the core of the Sun. Moreover, according to extensive experimental and theoretical studies, QGP demonstrates strongly coupled ideal liquid behavior, which directly contracts to the prediction from asymptotic freedom which predict such matter should behavior like a gas of weakly interacting quarks and gluons. Therefore, the inner workings and proper degrees of freedom of QGP must be somewhere in between weakly coupled quarks and gluons and color neutral hadrons because it still demonstrate significant color freedom due to deconfinement. However, the microscopic structure of QGP is still unknown. Currently, both experimental and theoretical efforts have been conducted to actively investigate the internal structure of QGP.

Based on its ideal liquid feature, QGP could be described by relativistic viscous hydrodynamics. In fact, the quantum limit predicted by the Anti-de-Sitter Space Conform Field Theory (AdS/CFT). It is about a factor of larger than water.

The accurate equation of state of QGP is currently unknown. According to MIT Bag Model, the energy density ϵ and pressure p of a plasma of free quarks and gluons as a function of temperature T is as follows [45]:

$$\epsilon = \frac{37\pi^2}{30}T^4 + \mathcal{B} \quad (1.14)$$

$$p = \frac{37\pi^2}{90}T^4 - \mathcal{B} \quad (1.15)$$

Here, \mathcal{B} is the Bag Constant, which can be understood as the pressure of the vacuum on the quarks and gluons to make them form hadrons with finite size.

If we represent p in terms of ϵ , we get

$$p = \frac{1}{3}(\epsilon - 4B) \quad (1.16)$$

1.4.4 Color Superconductor

Under extremely high net baryon density, there is another hypothetical state of QCD matter named Color Superconductor where the color charges can move freely [46]. Similar to the Cooper Pair formation mechanism of electrons in metals, quarks, as fermions, pair up and bosonized into diquark, and undergo Bose-Einstein condensation [46]. The diquark condensate, carrying color charges, can move without resistance and thus demonstrate color superconductivity. It is believed that the color superconductor exists in the core of neutron stars where the net baryon chemical potential is high [47]. However, so far no color superconductor has been discovered in laboratory or astrophysical observations.

1.4.5 Phase Transition

As we increase the temperature, hadron resonance gas will undergo a phase transition into QGP. The chiral symmetry is restored from the phase transition of hadron resonance gas to QGP. However, the order of the phase transition from resonance hadron to QGP is still unknown. According to lattice QCD calculations, near zero baryon chemical potential ($\mu_B = 0$), the phase transition is a smooth cross over. However, at finite baryon chemical, it is believe that the phase is a first order phase transition according to different model calculations [48]. The hint of first order phase transition can be found in the softening equation of state in the cross over region [49]. However, currently, the order of phase transition from hadron resonance gas to QGP at high baryon chemical potential is still an open question.

1.4.6 Critical Point

If the theoretical predictions are correct, according to thermodynamics, there must be a critical point between the first order phase transition and the smooth crossover. Theoretical calculations predict that the critical point is $\mu_B = 350 - 700$ and $T_c \approx 160$ MeV [50]. Experimentally, the scale of the critical temperature may occur at $T_c \approx 175$ MeV from high moment analyses [51]. The research on critical point, a landmark in the QCD phase diagram, and the phase transition between QGP and hadron resonance gas are very important topics for physicists to understand the nature of QCD matters. The STAR Collaboration has carried out a Beam Energy Scan, both Phase I and II, at RHIC and plan to extend it to higher baryon chemical potential and lower temperature in the future Fixed Target Mode to search the critical point in the QCD phase diagram. However, so far efforts to search the precise locations of the critical point is still ongoing. The results are still inconclusive [?].

1.5 High Energy Nuclear Physics

1.5.1 Laboratories

In laboratories, physicist collider heavy nuclei at high energy to study QCD under extremely hot and dense condition.

1.5.2 Heavy-Ion Accelerators

1.5.3 Heavy-ion Physics Detectors

1.5.4 Stages of Heavy-Ion Collisions

1.5.5 Coordinates

1.5.6 Glauber Model

1.6 The Quest for the Quark-Gluon Plasma

1.6.1 Signatures

1.6.2 Discovery

1.6.3 Properties

1.6.4 Microscopic Structure

1.6.5 Open Questions

1.7 Hard Probes

1.7.1 Jets

1.7.2 Electroweak Probes

1.7.3 Heavy Quarks

1.8 Open Heavy Flavor Physics

1.8.1 Heavy Quark Diffusion

1.8.2 Heavy Quark Energy Loss

1.8.3 Heavy Quark Hadronization

1.8.4 Experimental Observables

Chapter 2

The CMS Detector

2.1 Overview

2.2 Triggers

2.2.1 L1 Hardware Trigger

2.2.2 HLT Trigger

2.3 Tracking System

2.3.1 Silicon Pixel Detector

2.3.2 Silicon Strip Detector

2.3.3 Tracking Algorithm

2.4 Muon System

2.5 Calorimeter System

2.5.1 ECAL

2.5.2 HCAL

2.5.3 Forward HCAL

Chapter 3

Experimental Procedures

3.1 Experimental Setup

3.2 LHC Heavy-Ion Run

3.3 Minimum Biased Trigger

3.4 Dimuon Trigger

3.5 Run Monitoring

3.6 Data Acquisition

Chapter 4

Technical Objects

4.1 Hits

4.2 Clusters

4.3 Tracks

4.4 Vertices

4.5 Muons

Chapter 5

Data Analysis

5.1 Analysis Strategies

5.1.1 Physics Goals

5.1.2 General Workflow

5.1.3 Technical Challenges

5.2 Global Event Observables

5.2.1 Total Number of Events

5.2.2 Centrality Definition

5.2.3 Number of Participants Nucleons

5.2.4 Number of Binary Collisions

5.2.5 Event Multiplicity

5.3 Monte Carlo Simulations

5.3.1 PYTHIA

5.3.2 Hydjet Embedding

5.3.3 EvtGen Package

Chapter 6

Conclusions

6.1 Comparison with Other Experiments and Theoretical Models

6.2 Physics Messages Discussion

6.3 Conclusions

6.4 Future Outlooks

Chapter 7

Other Studies

7.1 sPHENIX Heavy Flavor Physics Simulations

7.2 sPHENIX Electromagnetic Calorimeter Studies

7.3 EIC Electromagnetic Calorimeter R&D

Appendix A

Tables

Table A.1: Armadillos

Armadillos	are
our	friends

Appendix B

Figures

Figure B-1: Armadillo slaying lawyer.

Figure B-2: Armadillo eradicating national debt.

List of Symbols

\hbar	Reduced Planck constant
c	Speed of light in a vacuum inertial frame
p_T	Transverse momentum
R_{AA}	Nuclear Modification Factor
CERN	European Center for Nuclear Research
CMS	Compact Muon Solenoid
LHC	Large Hadron Collider

Abbreviations

\hbar	Reduced Planck constant
c	Speed of light in a vacuum inertial frame
p_T	Transverse momentum
R_{AA}	Nuclear Modification Factor
CERN	European Center for Nuclear Research
CMS	Compact Muon Solenoid
LHC	Large Hadron Collider

References

- [1] M. K. Gaillard, P. D. Grannis, and F. J. Sciulli, “The Standard Model of Particle Physics”, *Rev. Mod. Phys.* 71 (1999)
- [2] C. D. Roberts, “Nonperturbative effects in QCD at Finite Temperature and Density”, *Phys. Part. Nucl.* 30 (1999)
- [3] P.A. Zyla et al. (Particle Data Group), “Review of Particle Physics”, *Prog. Theor. Exp. Phys.* 2020, 083 C01 (2020)
- [4] J. Gross and F. Wilczek, “Ultraviolet behavior of non-abelian gauge theories”, *Phys. Rev. Lett.* 30, 1343 (1973)
- [5] S. Dürr et al. "Ab Initio Determination of Light Hadron Masses", *Science*. 322 (5905): 1224 7 (2008)
- [6] N. Fettes, U.-G. Meißner, and S. Steininger, “Pion-nucleon scattering in chiral perturbation theory I: Isospin-symmetric case”, *Nucl. Phys. A* 640 (1998)
- [7] J. C. Collins, D. E. Soper, and G. F. Sterman, “Factorization of Hard Processes in QCD”, *Adv. Ser. Direct. High Energy Phys.* 5 (1989)
- [8] Francesco Becattini, “What is the meaning of the statistical hadronization model?”, *J. Phys. Conf. Ser.* 5 (2005)
- [9] B. Andersson, G. Gustafson, G. Ingelman, and T. Sjöstrand, “Parton fragmentation and string dynamics”, *Phys. Rep.* 97 (1983)

- [10] R. J. Fries, V. Greco, and P. Sorensen “Coalescence Models For Hadron Formation From Quark Gluon Plasma”, *Ann. Rev. Nucl. Part. Sci.* 58 (2008)
- [11] F. Wilczek, “QCD In Extreme Conditions”, Contribution to: 9th CRM Summer School: Theoretical Physics at the End of the 20th Century, 567-636
- [12] E. d’Enterria, David G., et al., “CMS physics technical design report: Addendum on high density QCD with heavy ions”, *J. Phys.G* 34 (2007)
- [13] E. Altman, “Many-body localization and quantum thermalization”, *Nat. Phys.* 14, 979 - 983 (2018).
- [14] M. P. Heller, R. A. Janik, and P. Witaszczyk, “Characteristics of Thermalization of Boost-Invariant Plasma from Holography”, *Phys. Rev. Lett.* 108, 201602 (2012)
- [15] G. Parisi, “Some considerations on the Quark-Gluon Plasma”, *Quark Matter 2018 Conference* (2018)
- [16]
- [17] H.C. Chandola, G. Punetha, and H. Dehnen, “Dual QCD thermodynamics and quark-gluon plasma”, *Nucl. Phys. A* 945 (2016)
- [18] R. Stock, “Relativistic Nucleus-Nucleus Collisions and the QCD Matter Phase Diagram”, In **Landolt-Boernstein I 21A: Elementary particles** 7
- [19] T.D. Lee and G.C. Wick, “Vacuum stability and vacuum excitation in a spin-0 field theory”, *Phys. Rev. D* 9 2291(1974)
- [20] H. S. Chung, J. Lee, and D. Kang, “Cornell potential parameters for S-wave heavy quarkonia”, *J. Korean Phys. Soc.* 52 (2018)
- [21] J. Harris and B. Muller, “The Search for the quark-gluon plasma”, *Ann. Rev. Nucl. Part. Sci.* 46 (1996)
- [22] J.O. Andersen and T. Brauner, “Linear sigma model at finite density in the $1/N$ expansion to next-to-leading order”, *Phys .Rev. D* 78:014030 (2008)

- [23] M. Asakawa and K. Yazaki, “Chiral Restoration at Finite Density and Temperature”, Nucl. Phys. A 504 (1989)
- [24] K. Fukushima, D.E. Kharzeev, and H.J. Warringa, “The Chiral Magnetic Effect”, Phys. Rev. D 78 074033 (2008)
- [25] S. Shi, H. Zhang, D. Hou, and J. Liao, “Signatures of Chiral Magnetic Effect in the Collisions of Isobars”, Phys. Rev. Lett. 125 (2020)
- [26] J. Zhao and F-Q. Wang, “Experimental searches for the chiral magnetic effect in heavy-ion collisions”, Prog. Part. Nucl. Phys. 107 (2019)
- [27] D.E. Kharzeev, J. Liao, S. A. Voloshin, and G. Wang, “Chiral Magnetic and Vortical Effects in High-Energy Nuclear Collisions — A Status Report”, Prog. Part. Nucl. Phys. 88 (2016)
- [28] S. Choudhury, G. Wang, W. He, Y. Hu, and H.Z. Huang, “Background evaluations for the chiral magnetic effect with normalized correlators using a multiphase transport model”, Eur. Phys. J. C 80 (2020)
- [29] R. Hagedorn, “Statistical thermodynamics of strong interactions at high energies”, Nuovo Cim. , Suppl. 3 (1965)
- [30] J. Rafelski, “Melting Hadrons, Boiling Quarks”, from Hagedorn Temperature to Ultra-Relativistic Heavy-Ion Collisions at CERN. Springer, Cham.
- [31] C.A. Dominguez, “Color Deconfinement in QCD at Finite Temperature”, Nucl. Phys. B Proc. Suppl. 15 (1990)
- [32] K. Rajagopal and F. Wilczek, “The Condensed matter physics of QCD”, part of At the frontier of particle physics. Handbook of QCD. Vol. 1-3 (2000)
- [33] M.B. Gay Ducati, “High Density QCD”, Braz. J. Phys. 31 (2001)
- [34] D.E. Kharzeev, “Hot and dense matter: from RHIC to LHC: Theoretical overview”, Nucl. Phys. A 827 (2009)

- [35] L.D. McLerran, S. Schlichting, S. Sen, “Space-Time Picture of Baryon Stopping in the Color-Glass Condensate”, *Phys. Rev. D* 99, 074009 (2019)
- [36] F. Gelis, E. Iancu, and J. Jalilian-Marian, R. Venugopalan “The Color Glass Condensate”, *Ann. Rev. Nucl. Part. Sci.* 60 (2010)
- [37] J Jalilian-Marian and X.N. Wang, “Small x gluons in nuclei and hadrons”, *Phys. Rev. D* 60, 054016 (1999)
- [38] V.P. Gonçalves “QCD at high parton density”, *Braz. J. Phys.* 34 (2004)
- [39] F. Arleo and T. Gousset, “Measuring gluon shadowing with prompt photons at RHIC and LHC”, *Phys. Lett. B* 660 (2008)
- [40] P. Huovinen and P. Petreczky , “QCD Equation of State and Hadron Resonance Gas”, *Nucl. Phys. A* 837 (2010)
- [41] N. Sarkar and P. Ghosh , “van der Waals hadron resonance gas and QCD phase diagram”, *Phys. Rev. C* 98, 014907 (2018)
- [42] Jamal. Jalilian-Marian and X.N. Wang, “Shadowing of gluons in perturbative QCD: A comparison of different models”, *Phys. Rev. D* 63, 096001 (2001)
- [43] E. Epelbaum, H.-W. Hammer, and U.G. Meißner, “Modern theory of nuclear forces”, *Rev. Mod. Phys.* 81 (2009)
- [44] J. Rafelski, "Connecting QGP-Heavy Ion Physics to the Early Universe“, *Nucl. Phys. B Proc. Suppl.* 243-244 (2013)
- [45] S. M. Sanches Jr., F. S. Navarra, and D. A. Fogaça, “The quark gluon plasma equation of state and the expansion of the early Universe”, *Nucl. Phys. A* 937 (2015)
- [46] M. G. Alford, K. Rajagopal, T. Schaefer, A. Schmitt “Color superconductivity in dense quark matter”, *Rev. Mod. Phys.* 80 (2008)

- [47] M. G. Alford, “Color superconducting quark matter”, *Ann. Rev. Nucl. Part. Sci.* 51 (2001)
- [48] K. Rajagopal, “Mapping the QCD phase diagram”, *Nucl. Phys. A* 661 (1999)
- [49] G. Odyniec on behalf of STAR Collaboration, “Beam Energy Scan Program at RHIC (BES I and BES II) – Probing QCD Phase Diagram with Heavy-Ion Collisions”, *PoS CORFU2018* (2019)
- [50] Z. Fodor and S.D. Katz, “Critical point of QCD at finite T and μ , lattice results for physical quark masses”, *JHEP* 04 050 (2004)
- [51] S. Gupta, X. Luo, B. Mohanty, H. G. Ritter, N. Xu, “Scale for the Phase Diagram of Quantum Chromodynamics”, *Science* 332 (2011)